

Supporting material for

# Broadband spectrometer with single-photon sensitivity exploiting tailored disorder

*Wladick Hartmann<sup>1,2,\*</sup>, Paris Varytis<sup>3,4</sup>, Helge Gehring<sup>1,2</sup>, Nicolai Walter<sup>1,2</sup>,*

*Fabian Beutel<sup>1,2</sup>, Kurt Busch<sup>3,4</sup>, Wolfram Pernice<sup>1,2,\*</sup>*

<sup>1</sup>University of Münster, Institute of Physics, Wilhelm-Klemm-Str. 10, 48149 Münster, Germany

<sup>2</sup>University of Münster, CeNTech-Center for Nanotechnology, Heisenbergstr.11, 48149 Münster, Germany

<sup>3</sup>Max-Born-Institut, Max-Born-Str. 2A, 12489 Berlin, Germany

<sup>4</sup>Humboldt University Berlin, Institute of Physics, Theoretical Optics & Photonics, Newtonstr.15, 12489 Berlin, Germany

## S1 Measurement setup

After fabrication, the chip is placed on a 4-axes nano positioner (attocube systems AG) inside a closed-cycle cryostat, in which the sample is cooled down to 1.3 K. To launch light into the chip, we use 16 standard SMF-28 fibers assembled in a fiber array with 127  $\mu\text{m}$  pitch. We use alignment structures composed of two couplers connected with a waveguide which are placed to the left and right of the main input of our device. The position of the spectrometer with respect to the fiber array is optimized by maximizing the transmission through these alignment structures using a tunable laser source (NewFocus TLB 6600) and an HP 8163A power meter with an HP 81634B InGaAs power sensor module. The electrical connection to the detectors is established with a multi-contact Unity probe from FormFactor. For biasing the detectors at a current of 80% of their switching current we employ a low noise current source (Keithley 2400). The readout of the RF signal is realized with a high-speed time tagger (Ultra, Swabian Instruments).

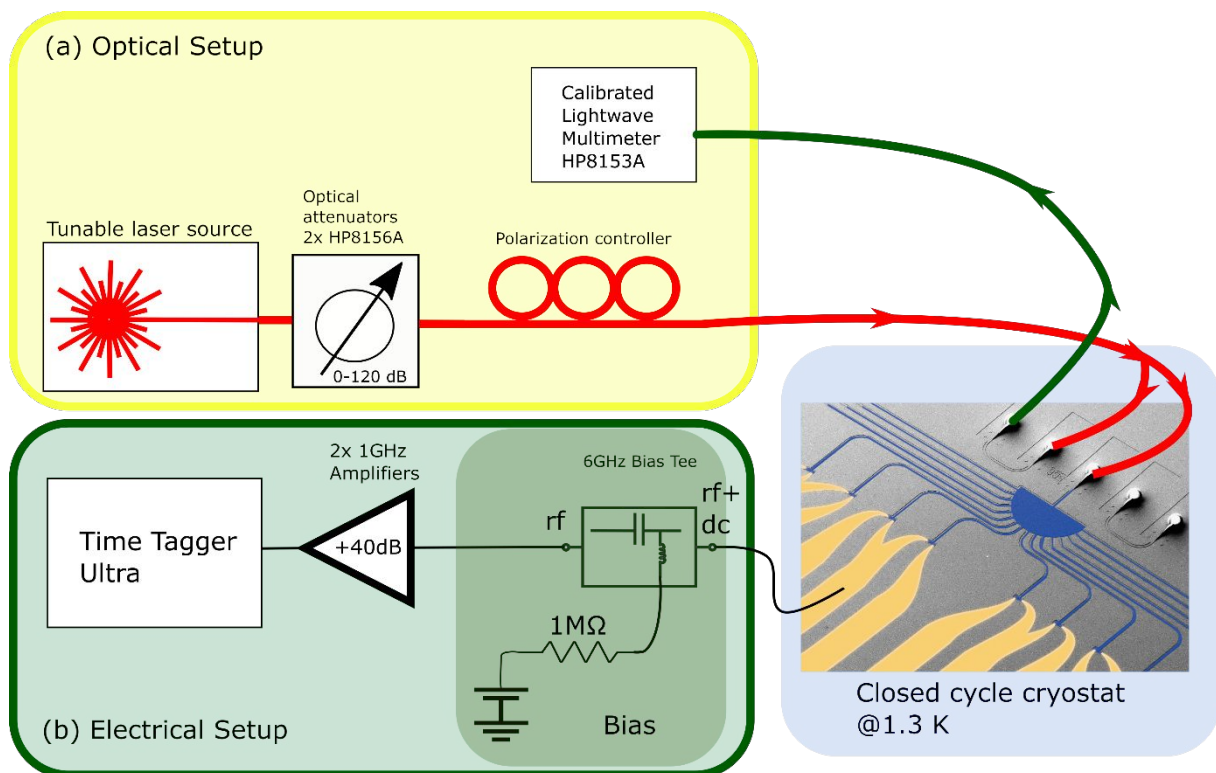


*Figure S 1 Schematic representation of the measurement setup. (a) depicts the optical setup with a tunable laser source (TLB 6700 and TLB 6600), two variable optical attenuators in series and a polarization controller. Light is coupled to the chip via a fiber array (not depicted). (b) Electrical setup. A UnityProbe with 8 RF contacts is used for electrical connection of the SNSPDs. The detector is biased by a stable source (Keithley 2400) and the output signal is registered by a time tagging device from Swabian Instruments after being amplified by low noise amplifiers (mini circuits ZFL-1000LN+).*

Because the electrical probe allows only for 8 RF contacts, the measurement of our device with a total of 16 detectors has to be performed in two steps, by measuring the first 8 detectors and then moving to the next 8 detectors. Since in our setup the chip is being moved with the nano positioner, while the fiber array and the RF probe stay fixed, moving the chip to the second row of detectors means that the input fiber to the device also changes. In other words, for the first row of detectors, the optical input signal is provided by the first fiber in the 16 channel fiber array, while for the second row the chip is moved such, that the 12th fiber launches the light into the device. Obviously, in order to move the chip, it has to be electrically disconnected by moving the chip down in z-direction. Therefore, in this

particular setup, we have to record the transmission of any probe signal through the device to each detector right after recording the transmission of the calibration signal, in order to ensure no change in polarization.

Figure S 1 depicts schematically the used setup. Two different tunable laser sources are used for both the recording of the transmission matrix as well as the probe signal in the wavelength ranges of 1500-1600 nm and 793-808 nm. The light is attenuated by two variable optical attenuators, the polarization can be controlled with a three paddle polarization controller before being launched through a fiber array onto the chip. A calibrated multimeter is used for reference measurement through the reference waveguides next to the main device.

In order to record the transmission for a known spectrum through the device we use the internal sweeping functions of each respective laser source. For the wavelength range from 1530 nm to 1580 nm we sample the detector response 2000 times with an integration time per sampling point of 5 ms, leading to a discretization of 25 pm between each sampling point. For 793 nm to 808 nm we sample 1500 times with a detector integration time of 20 ms, leading to a wavelength difference between neighboring sampling points of only 10 pm.

## S2 Insertion loss

In the main text we discuss the reconstruction of heavily attenuated signals. In order to determine the exact power which is actually launched into the scattering area, we first measure the back-to-back transmission through the setup (laser -> attenuators -> pol controller -> power meter) which is depicted in Figure S 2 as the black curve (Insertion Loss). We then measure the same spectrum through a reference waveguide on the chip (polymer coupler – waveguide – polymer coupler) to determine the coupling losses of our polymer couplers (blue curve). Since in this measurement the waveguide between the couplers is only around 130  $\mu\text{m}$  long, we can neglect propagation losses and therefore the transmission spectrum through the reference waveguide is composed of the overall fiber losses (mostly the insertion loss of the two optical attenuators) and the insertion loss of both polymer couplers at each end of the reference waveguide. Therefore, we can determine the exact input power, launched into the scattering area of our spectrometer (green curve), which is exactly -21.5 dBm for 1550 nm.

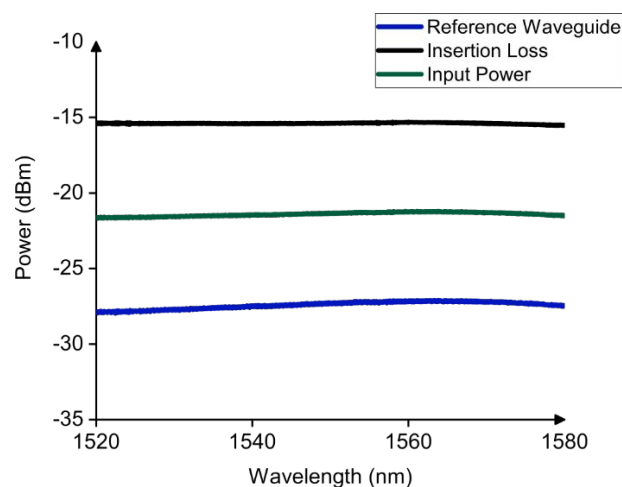


Figure S 2 Reference measurements for determining the insertion loss into the scattering area for the near-IR range. The black curve depicts the transmission through the optical setup without the fiber array, the blue curve the transmission through a reference waveguide device next to the spectrometer and the green curve the thus determined actual transmission into the scattering area.

### S3 Detector speed

Figure S 3 depicts a typical voltage response of one of our SNSPDs, recorded with an oscilloscope. When a photon is absorbed, the superconductivity inside the nanowire breaks down, leading to voltage pulse due to the bias current inside the nanowire. The rising time of such pulse is in the picosecond time frame, while the relaxation takes several nanoseconds (exponential decay). Generally speaking, the detector deadtime, thus the time in which the detector is blind for any incoming photons after a detection event, is the time after which the voltage pulse has decreased to a level of  $1/e$ . In our case this is around 10 ns. Thus, the detection speed of our detector is around 100 MHz.

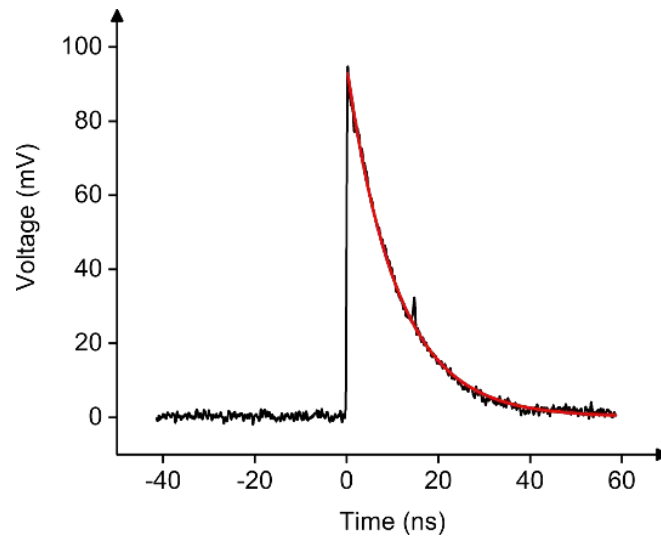


Figure S 3 Oscilloscope trace of a single click of the SNSPD. Black curve actual curve from oscilloscope averaged over 16 traces. Exponential fit in red.

### S4 Detector I-V characteristics

For a device with many SNSPDs it is desirable that all detectors exhibit similar properties. One of those properties is the switching current, at which the detector switches from superconducting to normal state. In our experiment, we bias every detector at 80% of its switching current. The switching current is determined by measuring an IV-curve of each detector. Due to the  $1\text{ M}\Omega$  series resistor in our setup, 1 V corresponds to exactly  $1\text{ }\mu\text{A}$  on our detector. When the switching current is reached, the current drops, because the resistivity of the detector increases from  $0\text{ }\Omega$  to a final number. Figure S 4 a) depicts such IV-curves for all measured 16 detectors of our spectrometer. The thus determined switching current  $I_c$  is depicted in b). Over all 16 detectors the switching current remains reasonably stable.

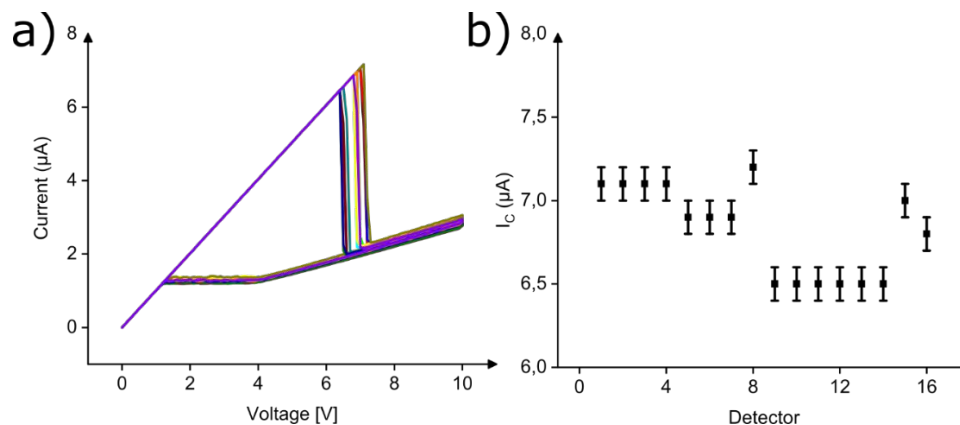


Figure S 4 a) IV curves for all 16 detectors. b) switching currents  $I_c$  for each detector.

## S5 Repeatability of spectral-to-spatial mapping

In order to quantify the repeatability of our transmission matrix measurement and thus the stability of our detectors in terms of clicks per wavelength, we perform the transmission measurement for each detector multiple times. We therefore collect 30 transmission matrices for our device and calculate the standard deviation of the measurements. A heatmap representation of the standard deviation is presented in Figure S 5. As in the main text, the center detectors in the heatmap (5-12) represent the detectors at the center of the actual device (mostly forward scattering) while detectors 1-4 and 13-16 represent the peripheral detectors of the device. It is clearly shown, that the uncertainty for the peripheral detectors becomes higher, since also the absolute number of photons reaching those detectors and therefore the signal-to-noise ratio is smaller. However, we determine the mean uncertainty over the entire matrix to 2.95%, with a lowest at 0.3% and the highest at 13.2%. We would like to stress that these transmission measurements were performed with a detector integration time of 5 ms per wavelength. A higher integration time would ensure higher number of clicks per detector and therefore smaller uncertainty, as is the case for the centered detectors.

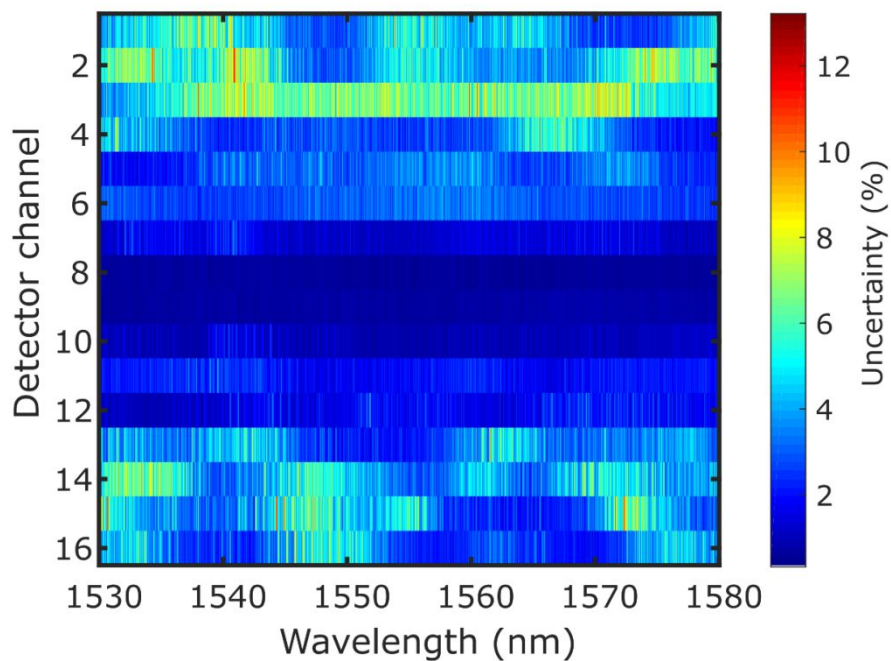


Figure S 5 Heatmap representation of the standard deviation of a transmission matrix measured over 30 times.

## S6 Matlab calculations for the broadband capability and dependence on the number of detectors

As stated in the main text, the bandwidth which can be successfully reconstructed is limited to  $2D\delta\lambda$ , where  $D$  denotes the number of detectors and  $\delta\lambda$  the spectral resolution. Since our device only has 16 detector channels, we demonstrate the mentioned dependence of the bandwidth on the number of detectors by creating a random matrix with MatLab. We create five different matrices with 10, 20, 30, 40 and 50 detectors and a corresponding number of wavelengths between 1530 and 1580 nm. This means, that with 10 detectors our transmission matrix has only 10 wavelengths between 1530 and 1580 nm leading to a maximum resolution of 5 nm, whereas with 50 detectors we can already have a resolution of 1 nm provided the bandwidth stays 50 nm. In order to simulate the stronger forward scattering in our experimental devices, the MatLab generated matrix includes more detected power in the central channels. To demonstrate the reconstruction capabilities, we then extract from the

transmission matrix one column at a time (representing the transmission of a single wavelength through all detectors) and adding the column to the next one. Then, we multiply the result with a gaussian function. In this way, we synthesize the transmission of a gaussian signal through our MatLab generated device between 1530 and 1580 nm. We then use the transmission matrix to reconstruct this gaussian signal. **Error! Reference source not found.** depicts the 5 calculated matrices with the corresponding reconstruction of a gaussian signal. If we assume that the device has a spectral resolution of 1 nm, like our experimental results show for the case of visible light and the very near IR, 50 detectors are already sufficient to reconstruct a bandwidth of 50 nm with a resolution of 1 nm. In order to reconstruct a broader spectrum, one can either implement more detectors, which would be rather complex, or simply record a transmission matrix for the adjacent wavelength range. One could for instance record such a matrix for 900-950 nm and a second matrix for 950-1000 nm and a third matrix for 1000-1050 nm. By utilizing three different stored matrices one would achieve a bandwidth of 150 nm with only 50 spatial channels.

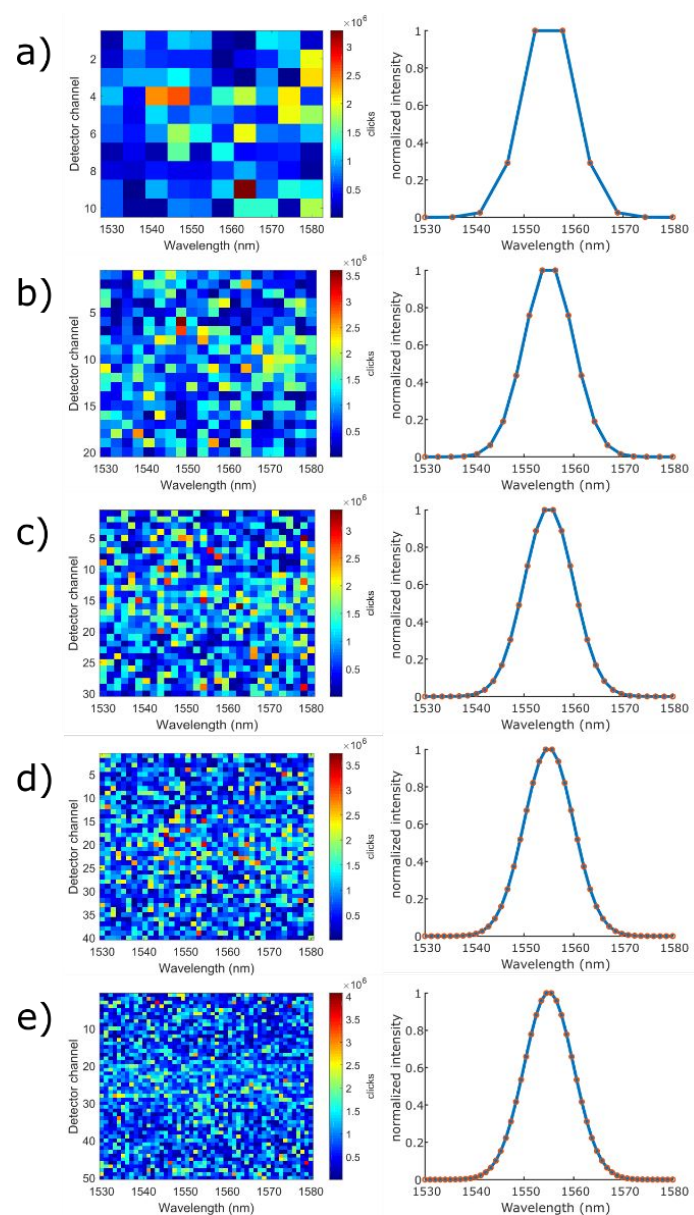


Figure S 6 Transmission matrices generated with MatLab for a) 10 detectors and up to e) 50 detectors. The transmitted power through each channel and wavelength is represented as photon counts (clicks). Next to each transmission matrix a reconstructed gaussian signal is depicted (blue line) with the original gaussian (red dots).

### S7 Waveguiding of TE- and TM-mode

As mentioned in the main text, the coupling efficiency of light to the waveguides by use of the 3D couplers is polarization dependent only if the waveguide does not support a certain polarization. In our case, we use Silicon Nitride waveguides of 330 nm height and 1.3  $\mu\text{m}$  width. This geometry does support the guiding of both TE- and TM- polarized light at 1550 nm wavelength as depicted in **Error! Reference source not found.**, however the mode TM- polarized light is leaking heavily into the oxide underneath the waveguiding material. With decreasing wavelength however, the confinement of the mode will improve, such that TE- and TM- guiding of light with lower wavelengths than 1550 nm is equally possible.

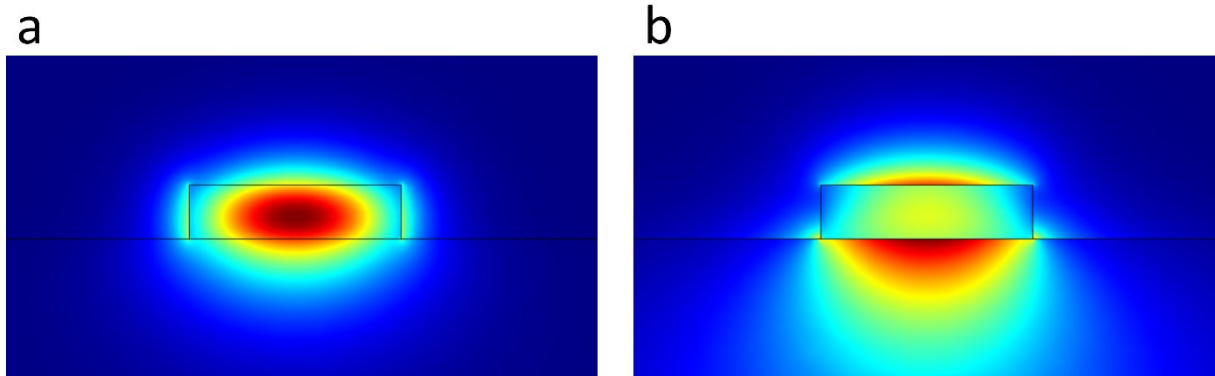


Figure S 7 Mode analysis using COMSOL for a) TE- and b) TM-polarized light at 1550 nm wavelength.

### S8 Signal-to-noise ratio

Figure S 8 depicts the measured signal-to-noise ratios for the four signals, presented in the main text. Since all signals were measured with an integration time of the detectors being 60 s, the SNR is calculated by taking the ratio of the each detector count and the dark counts, based on the dark count rate of 1 Hz.

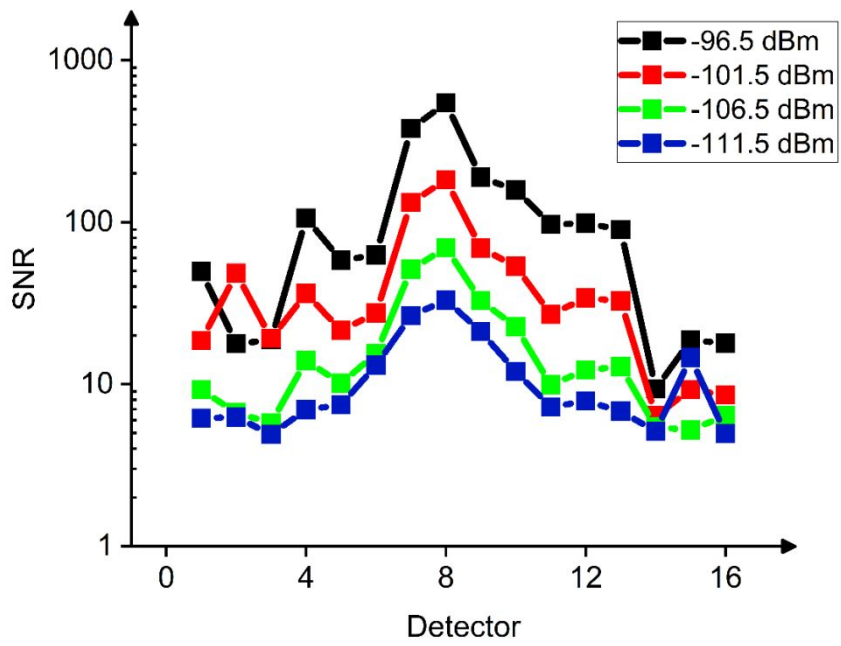


Figure S 8 Signal to noise ratio of the 16 detectors for a probe signal at 1550 nm wavelength in dependence of input power

**S9 Fabrication**

The width of the waveguides has been designed to be 1.3  $\mu\text{m}$  and a linear taper to 2.5  $\mu\text{m}$  is implemented at the outcoupling of the scattering region in order to increase the light collection area. The superconducting single-photon detectors are arranged in U-shaped nanowires made of 4 nm thick niobium nitride (NbN) sitting atop the nanophotonic waveguide. Each nanowire is connected to gold contact pads, which are used for electrical readout of the detectors. The detectors are 80  $\mu\text{m}$  long and 100 nm wide. Because of the employed travelling wave geometry in which the evanescent field of the mode propagating inside the waveguide is coupled to the nanowire, high absorption efficiency is achieved.<sup>1</sup>

The layout has been designed by using our in-house python-based tool<sup>2</sup> and the complete chip is fabricated in a top-down approach. We start with a silicon substrate with 3.3  $\mu\text{m}$  buried oxide (BOX), a 330 nm layer of  $\text{S}_3\text{N}_4$  and a 4 nm layer of NbN. In a first step, the gold contact pads together with alignment markers are fabricated by employing electron beam lithography with positive tone resist (PMMA 950K 4.5) with subsequent metal evaporation and lift-off. In the second step we pattern the nanowires using negative tone resist (HSQ 6%), e-beam lithography and reactive ion etching (RIE). Then, the nanophotonic waveguides and the scattering region are patterned using the positive tone resist AR-P 6200 and a further RIE step. Following fabrication of the planar structure, the 3D coupling structures are realized by additive manufacturing using direct laser writing (DLW) with a Nanoscribe tool (Nanoscribe Professional GT, 63x objective). These couplers achieve near-adiabatic fiber-to-waveguide coupling with broadband transmission characteristics<sup>3,4</sup>. By exploiting total internal reflection (TIR) our couplers provide good mechanical stability while maintaining a bandwidth of over 1000 nm and are compatible with cryogenic operation. At telecom wavelengths the couplers exhibit very low insertion losses of around 1.8 dB and an overall coupling efficiency above -8 dB over a broad wavelength range from 730 nm to 1700 nm. Furthermore, they allow for a relaxed mechanical alignment with respect to optical fibers, with -1 dB alignment tolerance of about 5  $\mu\text{m}$  in the x- and y-directions parallel to the chip surface and -1 dB alignment tolerance in the out-of-plane z-direction of 34  $\mu\text{m}$ . Additionally, the fabrication of many such 3D couplers with high yield is highly reproducible.

The waveguide geometry of 1.3  $\mu\text{m}$  width and 330 nm height was optimized for TE-polarized light at telecom wavelengths with a suppression of TM-modes by around 15-20 dB. However, with decreasing wavelengths both TE- and TM-modes are equally supported by the waveguides. Since the 3D couplers are almost not polarization dependent, both polarizations can be used in our spectrometer. However, the transmission matrix will change with polarization<sup>5</sup> and thus the transmission matrix must be recorded for the same polarization as the unknown spectrum. This matrix contains the transmission of every wavelength in the desired wavelength range through all output ports of the device. In contrast to traditional nanophotonic spectrometer designs, the random spectrometer is therefore robust against fabrication errors. Even though imperfections affect the speckle pattern and hence the absolute transmission characteristics of the device, the reconstruction of a probe signal is not impaired.

## References

- (1) Pernice, W. H. P.; Schuck, C.; Minaeva, O.; Li, M.; Goltsman, G. N.; Sergienko, A. V.; Tang, H. X. High-Speed and High-Efficiency Travelling Wave Single-Photon Detectors Embedded in Nanophotonic Circuits. *Nature Communications* **2012**, *3*, 1325. <https://doi.org/10.1038/ncomms2307>.
- (2) Gehring, H.; Blaicher, M.; Hartmann, W.; Pernice, W. H. P. Python Based Open Source Design Framework for Integrated Nanophotonic and Superconducting Circuitry with 2D-3D-Hybrid Integration. *OSA Continuum, OSAC* **2019**, *2* (11), 3091–3101. <https://doi.org/10.1364/OSAC.2.003091>.

- (3) Gehring, H.; Blaicher, M.; Hartmann, W.; Varytis, P.; Busch, K.; Wegener, M.; Pernice, W. H. P. Low-Loss Fiber-to-Chip Couplers with Ultrawide Optical Bandwidth. *APL Photonics* **2019**, *4* (1), 010801. <https://doi.org/10.1063/1.5064401>.
- (4) Gehring, H.; Eich, A.; Schuck, C.; Pernice, W. H. P. Broadband Out-of-Plane Coupling at Visible Wavelengths. *Opt. Lett., OL* **2019**, *44* (20), 5089–5092. <https://doi.org/10.1364/OL.44.005089>.
- (5) Varytis, P.; Huynh, D.-N.; Hartmann, W.; Pernice, W.; Busch, K. Design Study of Random Spectrometers for Applications at Optical Frequencies. *Opt. Lett., OL* **2018**, *43* (13), 3180–3183. <https://doi.org/10.1364/OL.43.003180>.